Biogeosciences
Open Access

Discussions

EGU

Physical and biogeochemical spatial scales of variability in the East Australian Current separation zone from shelf glider measurements

A. Schaeffer[1], M. Roughan[1], E. Jones[2], and D. White[1]

[1]Coastal and Regional Oceanography Lab, School of Mathematics and Statistics, University of New South Wales, Sydney NSW, 2052, Australia
[2]CSIRO Oceans and Atmosphere, Hobart, Tasmania, Australia

Correspondence to: A. Schaeffer (a.schaeffer@unsw.edu.au)

BGD

12, 20101–20121, 2015

Physical and biogeochemical spatial scales

A. Schaeffer et al.

Title Page

Abstract	Introduction
Conclusions	References
Tables	Figures

|◀ ▶|

◀ ▶

Back Close

Full Screen / Esc

Printer-friendly Version

Interactive Discussion

Abstract

In contrast to physical processes, biogeochemical processes are inherently patchy in the ocean, which affects both the observational sampling strategy and the representativeness of sparse measurements in data assimilating models. In situ observations from multiple glider deployments are analyzed to characterize spatial scales of variability in both physical and biogeochemical properties, using an empirical statistical model. We find that decorrelation ranges are strongly dependent on the balance between local dynamics and mesoscale forcing. The shortest horizontal (5–10 km) and vertical (45 m) decorrelation ranges are for chlorophyll *a* fluorescence. Whereas those variables that are a function of regional ocean and atmosphere dynamics (temperature and dissolved oxygen) result in anisotropic patterns with longer ranges along (28–37 km) than across the shelf (8–19 km). Variables affected by coastal processes (salinity and colored dissolved organic matter) have an isotropic range similar to the baroclinic Rossby radius (10–15 km).

1 Introduction

At the interface between oceanic and coastal processes, continental shelf regions are characterized by complex dynamics resulting from the interaction between different water masses at smaller spatial scales than the open ocean (Yoder et al., 1987). While wind, topography or density driven processes mostly influence the mixing and advection of the physical characteristics (temperature and salinity) of the shelf water masses, locally acting ecological processes are also determinant for biogeochemistry (Ballantyne et al., 2011). In particular, the numerous mechanisms driving phytoplankton distributions have been studied for many years, and highlight the complexity of these interactions (Martin, 2003). Biogeochemical (BGC) processes operate over a wide range of scales and thus need to be considered separately when investigating the dominant length scales of variability for the shelf water's properties (Pan et al., 2014).

The continental shelf off southeastern Australia (between 29 and 34° S) is relatively narrow, between 16 and 70 km (mean of 37 km) from the coastline to the 200 m isobath. The dynamics on the shelf are influenced both by local coastal processes and the episodic intrusion of the large scale East Australian Current (EAC) and its eddies (Fig. 1, Schaeffer et al., 2013, 2014a). The EAC is the western branch of the subtropical gyre in the South Pacific. It is a warm and dynamic poleward flowing current, encroaching on the continental shelf of southeastern Australia between 18° S (Ridgeway and Godfrey, 1994) and usually 30.7–32.4° S (Cetina-Heredia et al., 2014) where it bifurcates eastward, forming the Tasman Front. Further south, eddies are shed (Everett et al., 2012), leading to high variability in the velocity field and water masses on the shelf (Schaeffer et al., 2014b; Schaeffer and Roughan, 2015).

Previous studies have highlighted the high spatial heterogeneity of physical (Oke et al., 2008; Schaeffer and Roughan, 2015) and biochemical (Hassler et al., 2011) variables on this narrow shelf. De-correlation time scales were quantified from in situ mooring observations at 30 and 34° S (Roughan et al., 2013), being of the order of hours for across-shelf velocity to days and weeks for along-shelf flow and temperature, respectively. However, spatial scales of variability, which are essential for data assimilating models, have not been quantified.

Here we quantify for the first time the spatial scales of variability of both the physical and the BGC characteristics of the shelf water masses in the highly dynamic EAC separation zone. We use hydrographic measurements from 23 glider deployments along the coast (Sect. 2) to understand the variability amongst physical and BGC properties, the spatial anisotropy and the unresolved variance in the rich dataset (Sect. 3). Finally the results are discussed in the context of their applicability to modelling and data assimilation, where the perennial issue of relating point based measurements to model solutions is discussed (Sect. 4).

2 Methods

2.1 The dataset

Ocean gliders are autonomous underwater vehicles which use seawater to change their buoyancy, diving through the water column without using propulsion while record-
ing a wealth of scientific observations. Physical and biogeochemical measurements from 23 ocean glider deployments along the southeastern coast of Australia are used in this study. The glider missions span all seasons over 6 years, between 2008–2014, including results from both shallow-diving Slocum (< 200 m) and deep-diving Seaglider (< 1000 m) vehicles. The gliders were typically deployed at 29.4° S although some were
deployed as far south as 33° S (Fig. 1 and Schaeffer and Roughan, 2015). Missions range from 2–3 weeks to three months depending on the vehicle. The average horizontal displacement between two dives is around 200 m, while the fast sampling frequency leads to fine vertical resolution (< 2 m).

Scientific measurements include depth, temperature and salinity (from a Seabird-
CTD), dissolved oxygen (DO, from Aanderaa or Seabird Oxygen sensors), and optical parameters, chlorophyll *a* fluorescence (excited/emitted wavelengths: 470/695 nm), colored dissolved organic matter (CDOM, excited/emitted wavelengths: 370/460 nm) and backscatter coefficient at 650–700 nm (from a WETLabs optical sensor).

Quality control for physical parameters (temperature and salinity) and DO are con-
ducted following ARGO standards (Wong et al., 2014). For bio-optical parameters, quality control is more challenging due to the instrument bio-fouling and the high temporal and spatial variability of the measurements. Sensor drift is checked using pre- and post-deployment performance tests using purple and black solid standards and sensors are calibrated approximately every 2 years. The same tests are conducted
after cleaning the sensor from bio-fouling to check for sensor drift. These tests enable the identification and flagging of suspect measurements. A global range test is also conducted with a valid fluorescence maximum set to $50\,\mathrm{mg\,m^{-3}}$, similar to ARGO standards (Claustre, 2011). A valid regional maximum for CDOM is defined, based

on all the shelf glider deployments, as the mean plus 10 times the standard deviation (= 8.02 ppb) to remove high outliers (reaching 250 ppb).

2.2 Characterising spatial variability

The semivariogram approach was first introduced in geostatistics (Journel and Huijbregts, 1978) to characterize the spatial variability of a sparsely distributed dataset. It describes the average dissimilarity between measurements as a function of the distance separating them. This difference is generally small for measurements within close proximity, increasing with distance, until it does not depend on a spatial lag (decorrelated values) (Legaard and Thomas, 2007; Tortell et al., 2011).

For a variable anomaly $Z(x)$, the semivariogram or structure function, $\gamma(h)$, is defined as:

$$\gamma(h) = \frac{1}{2}\text{variance}[Z(x) - Z(x + h)] \tag{1}$$

where h is the distance separating the two observations in the x direction. In order to take into account outliers in the distribution of the empirical anomalies Z, Cressie and Hawkins (1980) proposed a robust estimate of the structure function:

$$\gamma(h) = \frac{\frac{1}{2}\left(\frac{1}{N}\Sigma[Z(x) - Z(x + h)]^{1/2}\right)^4}{0.457 + \frac{0.494}{N}} \tag{2}$$

where the sum is over all N pairs of measurements that are separated by the distance h.

The variables anomaly are obtained by removing large scale patterns, resulting from the average of all glider measurements over predefined bins determined by latitude and depth as in Schaeffer and Roughan (2015) and presented in details in a data descriptor (Schaeffer et al., 2015). This three-dimensional mean state is then smoothed using a spline method before being removed from each observation.

Both across- and along-shelf semivariograms are calculated to investigate anisotropy, where $h = \Delta x$ is the zonal distance, or $h = \Delta y$ is the meridional distance, respectively. The cross-shelf structure function is calculated following Eq. (2) from measurement pairs located within 0.1° of latitude. Similarly, the along-shelf structure $\gamma(h)$ is computed using observations within 0.1° of longitude from each other. In both cases the distance vector is discretized with intervals of 500 m and the time lag between pairs is limited to 1 day. The semivariograms are calculated in the horizontal plane at three depths: surface (0–5 m), mixed layer depth (MLD, 5–30 m, defined from the average profiles), or below the MLD at 50 m. Finally, glider profiles are also used to analyse vertical scales by computing $\gamma(h)$ with $h = \Delta z$ (intervals of 1 m).

The semivariance $\gamma(h)$ is computed from the trimmed mean (20 % outliers excluded) of measurements over all glider deployments, provided there are at least 10 different missions and more than 30 pairs for each spatial lag, to avoid seasonal bias or insignificant values. We then fit a spherical model (Doney et al., 2003) to the empirical semivariogram in order to extract the physical characteristics of the function, following:

$$
\begin{cases}
0 & h = 0 \\
\sigma_0^2 + (\sigma^2 - \sigma_0^2)\left(\frac{3}{2}\frac{h}{r} - \frac{1}{2}\left(\frac{h}{r}\right)^3\right) & 0 < h \leq r \\
\sigma^2 & h > r
\end{cases}
\tag{3}
$$

where h is the distance between measurements, σ^2 is the sill, σ_0^2 is the nugget and r the range. (These variables are described physically in the example below.) Exponential and Gaussian models (Biswas and Si, 2013) were also tested but were less adequate in terms of sum of squared error (sse) and adjusted R square statistics for the fit.

3 Results

3.1 Satellite derived SST semivariogram

By way of both example and validation we calculate the across-shelf semivariogram obtained from daily satellite remote sensed SST anomalies (Fig. 2). The spherical model
(Eq. 3) is fitted to the empirical semivariance values calculated for across-shelf lags over daily maps of SST in 2014. Only days with spatial coverage greater than 30 % of the domain are considered. The physical characteristics extracted from the model are indicated in Fig. 2. The sill σ^2 reflects the constant background variability of the variable. It is reached at a specific distance, here $r = 24$ km, which is referred to as the range or the dominant length scale. For lags greater than this range, the two observations are considered randomly correlated spatially. The nugget, σ_0^2, is the semivariance obtained from the model at the origin. If different from 0, it implies variability at shorter spatial scales than those resolved by the observations. This variability is either (a) real but unresolved, or (b) resulting from measurement or methodological errors. The semivariogram for SST (Fig. 2) shows very little nugget effect, showing the accuracy of the measurements and an adequate spatial resolution.

As expected, the semivariance of the SST anomaly (the annual mean was subtracted) differs with seasonality, as shown by the monthly empirical semivariograms (Fig. 2). Austral Summer and Autumn months are characterized by a sharper increase in the SST variance with greater variability in sills, due to more pronounced spatial temperature gradients. However, the range is similar, with dominant across-shelf scales between 18 and 32 km (not shown). The structure function reached a plateau for all months with the exception of January, suggesting a trend of longer scales (Yoder et al., 1987) and a limitation of the method.

3.2 Sill: in situ spatial variance

Semivariance values from glider measurements are analysed based on the values of the sill in each of the semivariograms shown in Fig. 3. Temperature, dissolved oxygen, and to a lesser extent colored dissolved organic matter (CDOM) and salinity, are characterised by a greater variance in the vertical than in the horizontal (see the different y axis). In contrast, chlorophyll a fluorescence shows comparable variability in all directions.

Focusing on horizontal sills (Fig. 3 middle and left), the highest variance for salinity and CDOM occurs at the surface in agreement with the influence of riverine input. The sill for DO is the greatest across-shelf and at 50 m than at the surface, suggesting more spatial variability due to bio-physical processes (remineralisation, respiration or bottom water uplift) than resulting from gas exchange with the atmosphere. Chlorophyll a fluorescence shows little variance at 50 m depth due to light limitation preventing biological activity. The highest horizontal sill for temperature appears below the MLD along the shelf, in agreement with the large latitudinal gradients in bottom temperature evidenced by Schaeffer and Roughan (2015). The surface temperature sill is smaller when measured by the gliders (Fig. 3) than by satellite (Fig. 2), possibly due to different measurement depth (in situ 0–5 m vs. skin SST), or seasonality, as glider deployments are more numerous in winter. Nevertheless, the across-shelf dominant length scales are in good agreement in the two datasets, with ranges of 25 and 19 km, respectively.

3.3 Range: in situ scales of variability

Across-shelf, along-shelf and vertical ranges are presented in Fig. 3 and summarized in Table 1. Spatial scales highlight different directional patterns between the parameters. Horizontal scales for salinity and CDOM are 9–15 km, 5–10 km for chlorophyll a, similar across and along the shelf. Mean temperature ranges across the shelf are 18–19 km at the surface and in the MLD, only 14 km at 50 m. Scales found along the shelf are greater, being 28–29 and 37 km, respectively. This directional anisotropy for tem-

perature is in agreement with the geometry of the shelf and the influence of the EAC at the shelf break (Fig. 1). Schaeffer and Roughan (2015) and Oke et al. (2008) both evidenced greater temperature gradients across than along the shelf, based on satellite, model and glider datasets. This directional anisotropy is also evident in density

5 (not shown), which has been shown to be mostly temperature driven (Schaeffer et al., 2014b), and even more intensified for DO. While DO is characterized by dominant across shelf scales similar to salinity and CDOM (8–15 km), the along-shelf spatial variability seems to be linked to the shallow EAC watermass, resulting in ranges of 27–35 km (surface and MLD) similar to temperature.

10 Chlorophyll *a* fluorescence has the smallest characteristic range both across and along the shelf, but also in the vertical. Measurements of fluorescence are decorrelated for depth lags greater than 46 m, in agreement with shallow (near surface) chlorophyll blooms. Vertical length scales for DO and CDOM (57–58 m), are less than those for temperature and salinity (62 and 66 m, respectively).

15 The second peak in vertical semivariance (at 80–100 m for temperature, salinity and DO, Fig. 3, right) indicates an anti-correlation for these lags (Legaard and Thomas, 2007). Negative correlation coefficients reaching -0.6 were previously observed from moored autumnal temperature observations in 100 m water depth at $-30°$ S (Roughan et al., 2013) and attributed to simultaneous heating source in the surface layers and

20 cooling at depth due to EAC encroachments and slope water uplift. Our results suggest that these current-driven uplifts are associated with a fresher and lower DO signature.

3.4 Nugget: in situ unresolved variance

The fraction of resolved and unresolved variance is estimated from the semivariogram parameters, the sill and nugget, respectively. A nugget occurs when the difference

25 between the two closest measurements is greater than 0, and can be seen at the origin of the semivariogram.

Overall, the high density glider observations capture most of the spatial ocean variability. The advantage of this sampling strategy is that nearly all the vertical variance

is resolved for most of the parameters (ratio $\sigma_0^2/\sigma^2 \sim$ 0–3 %, Table 1) due to the high sampling frequency of the gliders compared to their vertical displacement velocity. The only exception is for CDOM with the nugget being 24 % of the total variance (Fig. 3 and Table 1).

5   Horizontal variability is well resolved for temperature and salinity with ratios $\sigma_0^2/\sigma^2 \leq$ 10 % across the shelf, mostly ≤14 % along the shelf. Nuggets for BGC parameters are higher, especially for chlorophyll *a* fluorescence and CDOM measurements. While high nuggets for fluorescence can be attributed to horizontal sub-scale unresolved biological activity, CDOM datasets might suffer from measurement errors and quality control
10   issues as suggested by the high nugget effect in the vertical and the large outliers that had to be excluded (Sect. 2.1).

4   Discussion

This study combines in situ measurements from multiple glider deployments between 2008–2014 on the southeastern Australian continental shelf, to provide insight into the
15   surface and sub-surface structure of the water-mass dynamics, including the influence of the EAC, upwelling and freshwater inputs. Analysis of length-scale dependent variability demonstrates that much of the spatial variance in physical and BGC parameters typically occurs at scales ranging 5 km for chlorophyll *a* fluorescence to ∼ 35 km for along-shelf temperature.
20   In this study the length scales were averaged from data obtained over 2° of latitude, however we expect more regional variability resulting from the different latitudinal regimes evidenced by Schaeffer and Roughan (2015), driven by the meso-scale circulation. In addition, we expect that spatial scales may vary seasonally, particularly in the biological parameters. This will be tested when we have sufficient data in each season.
25   Uncertainties can arise from the semivariogram method, especially along the shelf where the data density is smaller. However, the results compare well when using dif-

ferent statistical fits, and are consistent with expected outcomes based on previous studies.

4.1 Related studies

From a global analysis of satellite derived surface data, Doney et al. (2003) found comparable small-scale variability for biology and physics. However, they were not able to characterize scales < 15 km based on the satellite products used. Here we find that BGC distribution occurs predominantly at submesoscales (5–15 km for chlorophyll *a*, CDOM), while scales for temperature are larger (18–37 km). These short scales of variability for BGC are in agreement with the effect of nutrient cycling, reproductive rate and community interaction (e.g. grazing pressure from zooplankton) that can lead to patches of 5–10 km (Ballantyne et al., 2011; Denman et al., 1977; Goebel et al., 2014).

According to Mahadevan and Campbell (2002), the fine scale patchy distribution of phytoplankton is linked to the short characteristic time in response to disturbance in their concentration, as opposed to the longer time for temperature to adjust to external forcing. We find temperature horizontal scales (18–37 km) that are of the same order of magnitude as over the Malvinas current region, derived from SST (20–47 km, Tandeo et al., 2014) or over the Middle Atlantic Bight from in situ glider observations (10–35 km, Todd et al., 2013). The anisotropic shape of the temperature variance is consistent with a highly dynamic circulation (Tandeo et al., 2014), here driven by the EAC, characterized by a greater signature in temperature than in salinity.

Spatial variability in salinity is predominantly isotropic and similar to CDOM with ranges of 9–15 km, corresponding to the first Rossby baroclinic radius of deformation (12–15 km based on local moored observation, Schaeffer et al., 2014b), and high surface variance, suggesting a predominant influence of coastal processes and river input.

4.2 Drivers of variability in a modelling perspective

Assuming that there is no first order feedback from the biology to the physics, we can think of the physics variables $\mathbf{X} = T, S$ (temperature and salinity) being a function of internal dynamics (I, e.g. mixing), atmospheric forcing (A), coastal buoyancy forcing arising from river discharge (R), friction due to shallow bathymetry (F), and open ocean forcing (e.g. tidal, geostrophy) and water masses (O). Therefore the state of the model at some spatial location "s" at time t is given by:

$$\mathbf{X}(s,t) = f(I,A,R,F,O) \tag{4}$$

where $f(I,A,R,F,O)$ for the physical variables can be solved numerically in various hydrodynamic models.

For the state variable of temperature, we assume that there is little effect from river input in this region (e.g. water coming in is about the same temperature as the surface layer), while the effect from coastal processes is large for salinity. Therefore Eq. (4) simplifies to:

$$T(s,t) = f(I,A,F,O) \tag{5}$$
$$S(s,t) = f(I,A,R,F,O) \tag{6}$$

Given that both T and S are subjected to the same advection and diffusion equations, but differ only in the source/sink and boundary terms of $f(A)$, $f(R)$ and $f(O)$, this is the major driver for the difference in the along shelf sills and differences in the nugget. Salinity varies over shorter length scales due to river input and the markedly different freshwater inputs from various catchment sizes along the coast. Whereas temperature is largely controlled by the regional scale EAC forcing and the relatively smooth atmospheric forcing applied which varies over spatial scales of 50 km or more.

A similar approach can be applied to the BGC variables, but $f(I)$ is more complicated as it includes the turnover of biomass/nutrients between different plankton functional types or nutrient pools. But ultimately, one would expect $f(I)$ to introduce variability at

scales equal to or less than those seen in salinity. This hypothesis is supported by the ranges reported in the chlorophyll *a* fluorescence and CDOM variables, which are biologically derived. However, as CDOM can also be introduced into the coastal ocean via river plumes and has a similar sill to salinity, we suggest that the CDOM measured by the glider is largely due to river discharge. The DO distribution in the surface layer is largely a function of air–sea exchange and will have similar variability to temperature due to the forcing mechanism. However, below the mixed layer, DO is function of the remineralisation rate and also vertical mixing/exchange with surface water, explaining the shorter range in DO found below the mixed layer.

4.3 Observing system design

The length scales calculated here can be used to guide the design of ocean observing systems. To answer questions related to the observation density needed to resolve along and across shore variability in both the physical and biological parameters. The temperature anisotropy in our results, consistent with findings of Oke and Sakov (2012) and Jones et al. (2015), shows that the required observation density will vary along and across the shelf. Thus high resolution across-shelf mooring or glider lines every Y km are more useful than simply a glider endurance line or equally spaced moorings. The distance Y can be initially derived from satellite observations, or determined after a number of glider missions. In contrast, the understanding of BGC variability, characterized by short isotropic length scales, will require high spatial resolution observations (e.g. gliders) to determine the representativeness of the measurements.

4.4 Data assimilation

The results from this study also allow us to partly answer the question of how to relate a point based observation with the output from a numerical model, which assumes the average concentration of a variable within a model cell X_{mod}. If we take a Bayesian view stating that we observe some true state variable with error (e.g. Parslow et al., 2013),

this can be written as:

$$X_{\text{obs}} = X_{\text{true}} + \epsilon_m + \epsilon_v \tag{7}$$

where X_{obs} is the observed variable, X_{true} is the true unknown value of the variable, ϵ_m is the instrument error and ϵ_v is the sampling error due to unresolvable small scale variability. The observation is then related to the modelled variable by:

$$X_{\text{mod}} = X_{\text{obs}} + \epsilon_r \tag{8}$$

where ϵ_r is typically referred to as the representation error (Oke and Sakov, 2008) associated with difference in kind (e.g. measuring fluorescence, but modelling biomass), or averaging across a model grid cell that contains a point measurement.

Assuming ϵ_m is known from calibration studies, results of studies like that presented here allow us to explore the characteristics of ϵ_v and ϵ_r. For a particular variable, we can assume that the nugget is approximately equal to ϵ_v and given a-priori information about a model grid, the spherical model applied to the semi-variogram can then be used to provide an empirical estimate not only for ϵ_r, but if observations are ingested into a data assimilation system, the estimates of the anisotropic range can be used to then tune the localization function (e.g. Oke et al., 2007) applied to each observation.

To this end, the results of this study allow us to characterise the length scales of the physical and BGC properties on the shelf and relate variability to the dynamical drivers, but additionally, the methodology developed here can be directly used to improve observing system design, and to tune key data assimilation parameters that are presently poorly understood.

References

Ballantyne, F., Schofield, O. M., and Levin, S.: The emergence of regularity and variability in marine ecosystems: the combined role of physics, chemistry and biology, Sci. Mar., 75, 719–731, 2011. 20102, 20111

Biswas, A. and Si, B. C.: Model averaging for semivariogram model parameters, in: Advances in Agrophysical Research, chapt. 4, 81–96, doi:10.5772/52339, 2013. 20106

Cetina-Heredia, P., Roughan, M., van Sebille, E., and Coleman, M. A.: Long-term trends in the east australian current separation latitude and eddy driven transport, J. Geophys. Res.-Oceans, 119, 4351–4366, doi:10.1002/2014JC010071, 2014. 20103

Claustre, H.: Bio-Optical Sensors on Argo Floats, Reports of the International Ocean-Colour Coordinating Group, no. 11, IOCCG. Tech. rep., IOCCG, Dartmouth, Canada, 2011. 20104

Cressie, N. and Hawkins, D.: Robust estimation of the variogram, J. Int. Ass. Math. Geol., 12, 115–125, doi:10.1007/BF01035243, 1980. 20105

Denman, K., Okubo, A., and Platt, T.: The chlorophyll fluctuation spectrum in the sea, Limnol. Oceanogr., 22, 1033–1038, doi:10.4319/lo.1977.22.6.1033, 1977. 20111

Doney, S. C., Glover, D. M., McCue, S. J., and Fuentes, M.: Mesoscale variability of sea-viewing wide field-of-view sensor (seawifs) satellite ocean color: global patterns and spatial scales, J. Geophys. Res.-Oceans, 108, 3024, doi:10.1029/2001JC000843, 2003. 20106, 20111

Everett, J. D., Baird, M. E., Oke, P. R., and Suthers, I. M.: An avenue of eddies: quantifying the biophysical properties of mesoscale eddies in the Tasman Sea, Geophys. Res. Lett., 39, L16608, doi:10.1029/2012GL053091, 2012. 20103

Goebel, N. L., Frolov, S., and Edwards, C. A.: Complementary use of wave glider and satellite measurements: description of spatial decorrelation scales in chl *a* fluorescence across the Pacific Basin, Meth. Oceanogr., 10, 90–103, doi:10.1016/j.mio.2014.07.001, 2014. 20111

Hassler, C., Djajadikarta, J., Doblin, M., Everett, J., and Thompson, P.: Characterisation of water masses and phytoplankton nutrient limitation in the east australian current separation zone during spring 2008, Deep-Sea Res. Pt. II, 58, 664–677, doi:10.1016/j.dsr2.2010.06.008, 2011. 20103

Jones, E. M., Doblin, M. A., Matear, R., and King, E.: Assessing and evaluating the ocean-colour footprint of a regional observing system, J. Marine Syst., 143, 49–61, doi:10.1016/j.jmarsys.2014.10.012, 2015. 20113

Journel, A. G. and Huijbregts, C. J.: Mining Geostatistics, Academic Press London, New York, x, 600, 1978. 20105

Legaard, K. R. and Thomas, A. C.: Spatial patterns of intraseasonal variability of chlorophyll and sea surface temperature in the California Current, J. Geophys. Res.-Oceans, 112, 006, doi:10.1029/2007JC004097, 2007. 20105, 20109

Mahadevan, A. and Campbell, J. W.: Biogeochemical patchiness at the sea surface, Geophys. Res. Lett., 29, 32-1–32-4, doi:10.1029/2001GL014116, 2002. 20111

Martin, A.: Phytoplankton patchiness: the role of lateral stirring and mixing, Prog. Oceanogr., 57, 125–174, doi:10.1016/S0079-6611(03)00085-5, 2003. 20102

Oke, P. and Sakov, P.: Assessing the footprint of a regional ocean observing system, J. Marine Syst., 105–108, 30–51, doi:10.1016/j.jmarsys.2012.05.009, 2012. 20113

Oke, P. R. and Sakov, P.: Representation error of oceanic observations for data assimilation, J. Atmos. Ocean. Tech., 25, 1004, doi:10.1175/2007JTECHO558.1, 2008. 20114

Oke, P. R., Sakov, P., and Corney, S. P.: Impacts of localisation in the EnKF and EnOI: experiments with a small model, Ocean Dynam., 57, 32–45, 2007. 20114

Oke, P. R., Brassington, G. B., Griffin, D. A., and Schiller, A.: The Bluelink ocean data assimilation system (BODAS), Ocean Model., 21, 46–70, doi:10.1016/j.ocemod.2007.11.002, 2008. 20103, 20109

Pan, C., Zheng, L., Weisberg, R. H., Liu, Y., and Lembke, C. E.: Comparisons of different ensemble schemes for glider data assimilation on West Florida Shelf, Ocean Model., 81, 13–24, doi:10.1016/j.ocemod.2014.06.005, 2014. 20102

Parslow, J., Cressie, N., Campbell, E. P., Jones, E., and Murray, L.: Bayesian learning and predictability in a stochastic nonlinear dynamical model, Ecol. Appl., 23, 679–698, 2013. 20113

Ridgeway, K. and Godfrey, J.: Mass and heat budgets in the East Australian Current: a direct approach, J. Geophys. Res., 99, 3231–3248, 1994. 20103

Roughan M., Schaeffer A., and Kioroglou S.: Assessing the design of the NSW-IMOS moored observation array from 2008–2013: Recommendations for the future OCEANS 2013 MTS/IEEE – San Diego: An Ocean in Common, 6741092, http://www.scopus.com/inward/record.url?eid=2-s2.0-84896371451&partnerID=40&md5=72cdf4718ce1086a3bf9ebdf3760cb05, 2013. 20103, 20109

Schaeffer, A. and Roughan, M.: Influence of a western boundary current on shelf dynamics and upwelling from repeat glider deployments, Geophys. Res. Lett., 42, 121–128, doi:10.1002/2014GL062260, 2015. 20103, 20104, 20105, 20108, 20109, 20110

Schaeffer, A., M. Roughan, and Morris, B.: Cross-shelf dynamics in a western boundary current. Implications for upwelling, J. Phys. Oceanogr., 43, 1042–1059, doi:10.1175/JPO-D-12-0177.1, 2013. 20103

Schaeffer, A., M. Roughan, and Morris, B.: Corrigendum cross-shelf dynamics in a western boundary current. Implications for upwelling, J. Phys. Oceanogr., 44, 2812–2813, doi:10.1175/JPO-D-14-0091.1, 2014a. 20103

Schaeffer, A., M. Roughan, and Wood, J. E.: Observed bottom boundary layer transport and uplift on the continental shelf adjacent to a western boundary current, J. Geophys. Res.-Oceans, 119, 4922–4939, doi:10.1002/2013JC009735, 2014b. 20103, 20109, 20111

Tandeo, P., E. Autret, B. Chapron, R. Fablet, and Garello, R.: SST spatial anisotropic covariances from METOP-AVHRR data, Remote Sens. Environ., 141, 144–148, doi:10.1016/j.rse.2013.10.024, 2014. 20111

Todd, R. E., Gawarkiewicz, G. G., and Owens, W. B.: Horizontal scales of variability over the Middle Atlantic Bight Shelf Break and continental rise from finescale observations, J. Phys. Oceanogr., 43, 222–230, doi:10.1175/JPO-D-12-099.1, 2013. 20111

Tortell, P., Gueguen, C., Long, M., Payne, C., Lee, P., and DiTullio, G.: Spatial variability and temporal dynamics of surface water pCO_2, $\Delta O_2/Ar$ and dimethylsulfide in the Ross Sea, Antarctica, Deep-Sea Res. Pt. I, 58, 241–259, doi:10.1016/j.dsr.2010.12.006, 2011. 20105

Wong, A., R. Keeley, and Carval, T.: Argo Quality Control Manual, Tech. rep., Argo Data Management Team, doi:10.13155/33951, 2014. 20104

Yoder, J. A., McClain, C. R., Blanton, J. O., and Oeymay, L.-Y.: Spatial scales in czcs-chlorophyll imagery of the southeastern U.S. Continental Shelf, Limnol. Oceanogr., 32, 929–941, doi:10.4319/lo.1987.32.4.0929, 1987. 20102, 20107

Table 1. Spatial scales of variability for spherical fit to robust structure functions for different parameters and depths across, along the shelf and along the vertical. The percentage ratio of the nugget to the sill (σ_0^2/σ^2) and R squared for the model fit to experimental values are also indicated (ranges with [*] correspond to R squared < 0.7). Blanks indicate unsuccessful fit to the spherical model.

|			Temperature	Salinity	Fluorescence	DO	CDOM
Across-shelf	Surface	range	19 km	13 km	5 km	10 km	10 km[*]
		ratio σ_0^2/σ^2	6 %	6 %	17 %	27 %	19 %
		R squared fit	0.96	0.94	0.89	0.85	0.49
	MLD	range	18 km	10 km	8 km[*]	8 km	14 km
		ratio σ_0^2/σ^2	4 %	0 %	13 %	18 %	2 %
		R squared fit	0.92	0.83	0.58	0.89	0.96
	50 m	range	14 km		5 km	15 km	11 km
		ratio σ_0^2/σ^2	10 %		15 %	4 %	17 %
		R squared fit	0.97		0.73	0.98	0.88
Along-shelf	Surface	range	29 km	15 km[*]	8 km	35 km	11 km[*]
		ratio σ_0^2/σ^2	14 %	14 %	20 %	2 %	21 %
		R squared fit	0.93	0.52	0.83	0.9	0.56
	MLD	range	28 km	10 km	10 km[*]	27 km	9 km[*]
		ratio σ_0^2/σ^2	8 %	23 %	21 %	18 %	10 %
		R squared fit	0.99	0.93	0.53	0.96	0.27
	50 m	range	37 km		5 km	4 km[*]	
		ratio σ_0^2/σ^2	1 %		8 %	5 %	
		R squared fit	0.97		0.87	0.33	
Vertical		range	62 m	66 m	46 m	58 m	57 m
		ratio σ_0^2/σ^2	0 %	3 %	1 %	0 %	24 %
		R squared fit	0.97	0.98	0.99	0.98	0.99
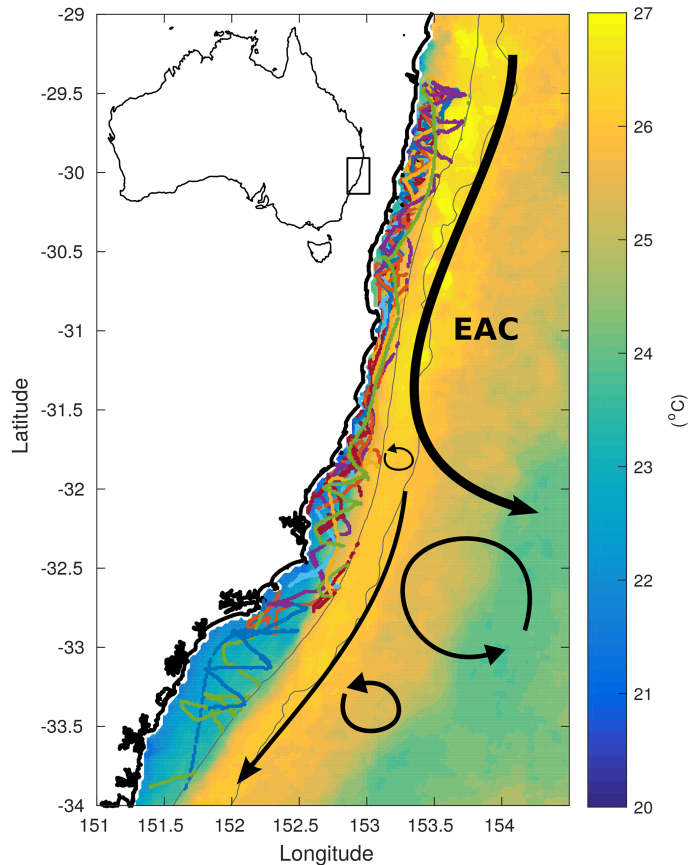
Figure 1. Monthly mean Sea Surface Temperature (GHRSST L3S product) over southeastern Australia for March 2014. The coastline, 200 and 2000 m isobaths are shown. Glider tracks over the shelf (depth < 200 m) are indicated by colored lines. A schematic of the typical circulation is shown with the poleward flowing East Australian Current bifurcating to the East around 32° S, its weaker extension, anticyclonic and cyclonic eddies.

Title Page

Abstract | Introduction

Conclusions | References

Tables | Figures

|◄ | ►|

◄ | ►

Back | Close

Full Screen / Esc
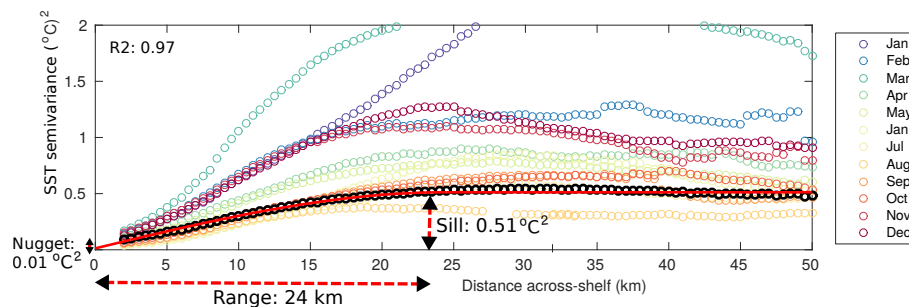
Printer-friendly Version

Interactive Discussion

Figure 2. Across-shelf empirical semivariogram estimated from daily SST over the southeastern Australian shelf (depth < 200 m, 29–34° S, GHRSST L3S product) for 2014 (black bold dots) and for each month in 2014 (colored dots). The spherical model (R^2 = 0.97 for the fit) and parameters (range, sill, nugget) are shown for 2014 semivariance.
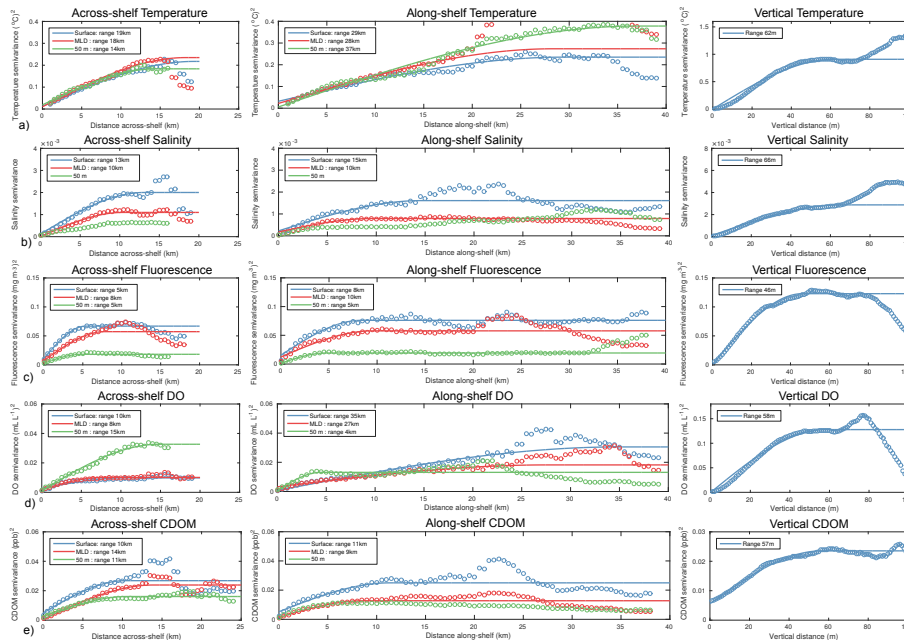
Figure 3. Across-shelf (left), along-shelf (middle) and vertical (right) empirical semivariograms estimated from glider measurements of **(a)** temperature, **(b)** salinity, **(c)** chlorophyll *a* fluorescence, **(d)** DO and **(e)** CDOM. Spherical models are shown by the solid lines and the resulting spatial ranges are indicated in the insert for successful fits. Blue, red, green symbols for horizontal semivariogram correspond to surface, MLD (0–30 m) and 50 m measurements, respectively.